JOURNAL OF CATALYSIS 96, 597–612 (1985)

Effects of Titania on the Coadsorption of H_2 and CO on Nickel Surfaces: Consequences for Understanding Methanation over Titania-Supported Nickel Catalysts

G. B. RAUPP AND J. A. DUMESIC

Department of Chemical Engineering, University of Wisconsin, Madison, Wisconsin 53706

Received March 22, 1985; revised July 22, 1985

The effects of titania adspecies on the coadsorption of CO and hydrogen on polycrystalline nickel were studied under ultrahigh vacuum conditions using temperature-programmed desorption. Titania blocks CO adsorption at strongly bound sites (desorption energies ~130 kJ · mol^{-1}) and enhances CO adsorption at more weakly bound sites (desorption energies ~90 kJ · mol^{-1}). In addition, the presence of titania on nickel increases the strength of hydrogen adsorption. This net weakening of CO adsorption and strengthening of hydrogen adsorption allows hydrogen to compete more effectively for nickel adsorption sites. Model calculations of this coadsorption behavior at temperatures and pressures representative of experimental methanation conditions (450–700 K and 0.1–10 kPa, respectively) showed that the measured changes in CO and hydrogen heats of adsorption on nickel should lead to a one to two order of magnitude increase in the H-adatom concentration for titania-containing surfaces. Assuming a mechanism wherein CO dissociation and carbon hydrogenation are balanced at steady state (neither step is rate limiting), this higher H-adatom coverage leads directly to a one to two order of magnitude higher methanation activity. Thus, the higher methanation activities of titania-supported nickel catalysts which exhibit so-called strong metal–support interactions can be understood in terms of more competitive hydrogen adsorption on the nickel surface.

INTRODUCTION

Since the original proposal several years ago that during high-temperature reduction titania species migrate onto the surfaces of titania-supported metal particles (e.g., *1–3*), evidence supporting this model has continued to grow (*4–11*). Recent work has concentrated on the study of model, or low-surface-area, unsupported metal catalysts containing titania adspecies; and, this has shown that the features of CO and H_2 chemisorption and/or CO hydrogenation typical of supported catalysts exhibiting so-called strong metal–support interactions (SMSI) can be reproduced for Ni (*5, 8, 10, 11*) and Pt (*9*).

For example, using temperature-programmed desorption (TPD) of CO and H_2 from a titania-containing polycrystalline nickel surface, Raupp and Dumesic (*8, 11*) showed that titania adspecies blocked CO adsorption and weakened the CO adsorption strength. In addition, hydrogen adsorption became activated. It was thought that creation of an activation energy barrier for dissociative hydrogen adsorption was responsible for the slow hydrogen uptakes previously observed for high-surface-area, titania-supported Ni and FeNi catalysts (*4*). Chung and co-workers (*5*) found a maximum in methanation activity over nickel at a titania coverage of 8% of a monolayer. The selectivity for the production of olefins from CO and H_2 over this surface (ethylene/methane ratio) was similar to that observed for nickel particles supported on $TiO_2\{100\}$.

If the presence of titania adspecies is responsible for the behavior of titania-supported metal particles, then an important remaining question is *how* these species lead to superior CO hydrogenation charac-

[1] Present address: Department of Chemical and Bio-Engineering, Arizona State University, Tempe, Ariz. 85287.

0021-9517/85 $3.00

teristics, as compared to the same metals on other supports. This is the subject of the present paper.

On the basis of the previous results which showed that titania surface species weaken CO adsorption and strengthen hydrogen adsorption on nickel surfaces (*8, 11*), one would expect the respective surface coverages of these two reactant species to be significantly different under steady-state CO hydrogenation conditions on a titania-containing Ni surface compared to a clean Ni surface. Vannice *et al.* (*12*) have attributed the higher CO hydrogenation activities for titania-supported catalysts to a weakened CO–metal bond, resulting in more competitive hydrogen chemisorption under reaction conditions. In this paper we present a study of the coadsorption of H_2 and CO on nickel surfaces under ultrahigh vacuum (UHV) conditions; these experiments establish the competitive nature of the coadsorption process. Using kinetic parameters determined in this study for adsorption and desorption of the two reactant species, mathematical models were developed which allowed estimation of the steady-state H and CO surface concentrations at methanation reaction temperatures (450–700 K) and moderate pressures (0.1–10 kPa). Based on these results, a model is presented to explain the role of titania surface species in CO hydrogenated reactions.

Coadsorption of H_2 and CO on single crystal Ni surfaces has been extensively studied. The wide variety of complementary techniques employed include TPD (*13–19*), work function measurements (*13, 15, 18*), ultraviolet photoemission spectroscopy (UPS) (*15, 17, 18*), X-ray photoelectron spectroscopy (XPS) (*18, 20*), low energy electron diffraction (LEED) (*13, 21*), high resolution electron energy loss spectroscopy (HREELS) (*13, 22*), and ion-induced desorption (*23*). These studies have been reviewed by White (*24*).

EXPERIMENTAL

Coadsorption of H_2 and CO on a clean, polycrystalline Ni surface and a titania-containing Ni surface was studied using temperature-programmed desorption in the UHV chamber described previously (*11, 25*). Hydrogen (Chemetron, 99.9%) and CO (Matheson, 99.5%) were dosed sequentially through separate dosing needles attached to independent manifolds. A constant heating rate of $\sim 20\ K \cdot s^{-1}$ was used throughout these studies. Multiplexing the mass spectrometer (UTI 100C) with a programmable peak selector allowed the desorption of CO and H_2 to be studied simultaneously. The desorption of potential hydrogenation products (e.g., CH_4) was also monitored. In this paper, coadsorption studies for a single coverage of titania, estimated to be ~0.2 monolayer (*11*) are reported. Experiments performed for different coverages gave results similar to those reported here.

RESULTS

Coadsorption on Clean Ni

Hydrogen and CO were coadsorbed at 130 K on the clean nickel surface by first exposing the polycrystal to 5 L H_2 (1 L = 1 Langmuir = 1.3×10^{-4} Pa · s) and then to varying CO exposure. During CO exposures, no H_2 was observed to desorb. The coadsorbed layer was then desorbed thermally. Desorption spectra are shown in Fig. 1. Exposure to 5 L H_2 and background CO, curves labeled a, resulted in negligible CO desorption and H_2 desorption from β_1 and β_2 states characteristic of clean nickel. Approximately 80% of the H-atom saturation coverage was achieved at that exposure. Carbon monoxide exposures from 0.5 to 3 L following H_2 exposure led to H_2 desorption at lower temperatures, as seen in curves b through d. A portion of the most strongly bound β_1 state is transformed to the weaker β_2 state. In addition, a third desorption state becomes evident as a shoulder on the low-temperature side of the desorption traces. Carbon monoxide desorption was apparently unperturbed by the presence of hydrogen at these low-CO, high-H initial coverages.

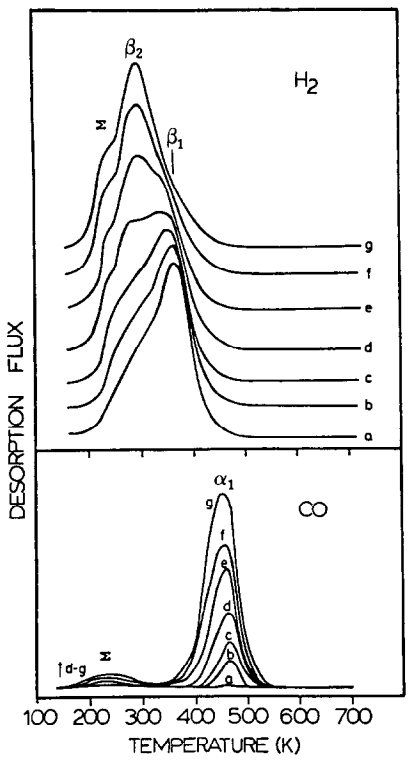

FIG. 1. Desorption flux of H_2 and CO coadsorbed on clean nickel. The sample was preexposed to 5 L H_2 at 130 K followed by (a) background, (b) 0.5, (c) 0.8, (d) 1.5, (e) 3.0, (f) 5.0, and (g) 10 L CO.

For CO exposures greater than 3 L, subsequent desorption (curves e–g) revealed a new CO-adsorption state. This state desorbs as a broad peak centered at 240 K, and it apparently corresponds to the low-temperature shoulder on the H_2 desorption traces. Similar peaks were first observed by Goodman *et al.* (*14*) following coadsorption of H_2 and CO on a Ni{100} surface and were designated Σ-states. The presence of Σ-states suggests that a strong adsorbate–adsorbate interaction exists under conditions of high-H and -CO surface concentration. This interaction does not take place on the more closely packed Ni{111} surface plane, as no Σ-states are created under similar conditions (*22, 24*).

Despite the apparent interaction between the coadsorbates H_2 and CO, no CO-hydrogenation products (e.g., methane) could be detected from the surface during heating. The presence of H preadsorbed on the polycrystalline Ni surface limited the saturation CO coverage to ~0.55 monolayer (1 monolayer ≡ 1.74×10^{19} m^{-2}), lower than the value of 0.67 monolayer achieved on the H-free surface. The more weakly bound α_2–CO states (desorption temperature 300–350 K) were nearly completely inhibited by hydrogen. Note that under these conditions H and CO in total amounts greater than 1 monolayer can be coadsorbed on the Ni surface.

The H_2/CO-coadsorption behavior on nickel under UHV conditions is a function of dosing order. Preexposure of the clean nickel surface to near-saturation doses of CO significantly inhibited the subsequent adsorption of hydrogen during H_2 exposure. For a CO coverage of 0.5 monolayer, the saturation H coverage achieved following 20-L exposure was only ~0.25, with a single observable desorption peak attributed to adsorption at β_2–H sites. No Σ-states were filled under these conditions, although the hydrogen-adsorption strength was somewhat weakened, as indicated by a moderate decrease in H_2-desorption temperature (by ~20 K).

These results favor a model previously proposed by Koel *et al.* (*15*) wherein CO and H compete for the same adsorption site corresponding to the most strongly bound states, α_1–CO and β_1–H. Since CO has a higher heat of adsorption, 2 H species are displaced from the β_1–H state to either the more weakly bound β_2–H states at intermediate CO exposures or to Σ-states at high CO exposures for each CO–α_1 state subsequently adsorbed. Since the Σ-states can be attributed to coadsorption in an intimately mixed adlayer in which both H and CO can be accommodated on a single site (*15, 24*) (see Discussion), total coverages greater than 1 monolayer can be achieved. When the order of absorption is reversed, filling of approximately one-half the α_1–CO states completely blocked subsequent adsorption of H_2 into the β_1 state.

Coadsorption on TiO_x/Ni

The presence of titania species on the

nickel surface markedly alters H_2/CO-coadsorption behavior, as shown in Fig. 2. This surface preexposed to 10 L H_2 at 130 K gave an initial H coverage near 80% of the saturation value, with desorption occurring from three states. The lower energy β_1 and β_2 states can be attributed to adsorption at Ni sites, whereas the highest energy state (labeled $\beta_2(TiO_x/Ni)$, desorbing at ~450 K) was created by the presence of titania. Subsequent adsorption of CO did not alter the H_2 desorption trace for CO coverages less than about 50% of the saturation value (exposures less than ~5 L). For higher CO coverages, β_1–H states are displaced to β_2–H. At saturation CO coverage, curve d, the β_1–H state is completely suppressed. The most strongly bound hydrogen state remains essentially unchanged by the presence of coadsorbed CO.

Consider next the desorption behavior of CO shown in Fig. 2. As discussed elsewhere (*11*), essentially three binding states are observed for CO on nickel surfaces containing titania. Two of these states, α_1(Ni) and α_2(Ni), are characteristic of CO on nickel sites while the third state, $\alpha_1(TiO_x/Ni)$, is observed only on nickel surfaces containing titania. These three states are labeled in Fig. 2. During these coadsorption studies, no Σ-states were observed in the region of the desorption spectra near 200–300 K. It is interesting to note, however, that the α_2(Ni)–CO and β_2–H states fill to greater populations than can be achieved when CO or H_2 are adsorbed alone, and that these states desorb at approximately the same peak temperature. These coadsorbed species may thus be coupled. Unlike the clean Ni surface, small amounts of CH_4 were evolved from the titania-containing nickel surface upon flashing. Methane desorbed as a broad (half-width ~ 100 K), low-intensity peak centered near 400 K. Desorption occurred via a reaction-limited process. The mass spectrometer was not calibrated for methane; assuming a sensitivity equal to that of hydrogen, the amounts of methane formed were in the range of 0.001–0.005 monolayer.

As for the clean Ni, no H_2 desorbed during CO exposures. Carbon monoxide saturation coverage was reduced to ~0.75 of the value attained in the absence of coadsorbed hydrogen. When the surface was first preexposed to CO to saturate the α_1(Ni) state, the subsequent adsorption of H_2 was markedly suppressed. The β_1–H state was completely blocked and the β_2–H state was partially blocked and slightly weakened. No Σ-states were observed. Fractional filling of the most strongly bound hydrogen state occurred despite the presence of strongly bound CO, and it appeared to displace a small amount of α_1(Ni)–CO to more weakly bound sites. This latter result is strong evidence that the $\beta_2(TiO_x/Ni)$ state of adsorbed hydrogen is, in fact, associated with nickel.

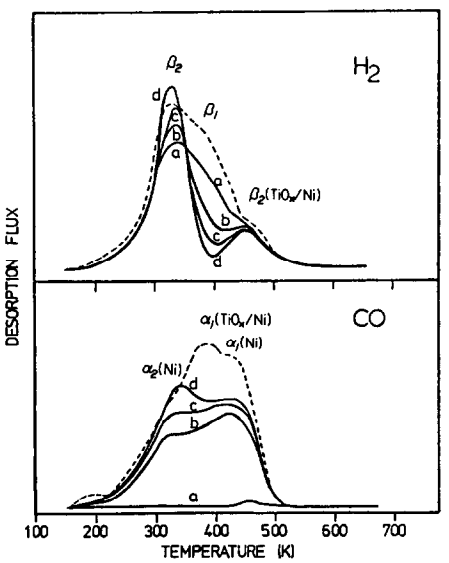

FIG. 2. Desorption flux of H_2 and CO coadsorbed on titania-containing Ni (θ_{Ti} ~ 0.2 monolayer). Solid curves are for 10 L H_2 adsorption at 140 K followed by (a) background, (b) 7, (c) 10, and (d) 20 L CO. Dashed lines correspond to desorption of a saturation layer of each gas adsorbed separately.

DISCUSSION

Coadsorption of H_2 and CO under UHV TPD Conditions

The TPD spectra for hydrogen and CO

coadsorbed at low temperature on the clean, polycrystalline Ni are in good agreement with those previously reported for Ni{111} and Ni{100} (*14–19, 24*). The Σ-states were typically filled to greater extents and desorbed as sharper peaks on the Ni{100} single crystal face than was presently observed for the polycrystalline surface. No low-temperature Σ-states are observed on Ni{111}. Comparison of H_2/CO coadsorption on other Group VIII metals such as Rh suggests that on close-packed {111} faces, repulsive interactions lead to segregation of CO and H, while on the more open {100} faces attractive interactions lead to mixing of CO and H (*24, 26, 27*). That sharper Σ-states were not observed on the polycrystalline Ni foil can be attributed to the structure of the foil, which most likely consists primarily of {100} and {111} exposed crystal planes.

Detailed spectroscopic characterization of the coadsorbed layer on Ni{100} has led to a coherent picture of the nature of the CO/H interaction. UPS (*15*) and HREELS (*22*) measurements have revealed that, below the desorption temperature of the Σ-states, no C–H or O–H bonds are formed in the coadsorbed layer. XPS (*18*) and HREELS (*22*) analyses have suggested, however, that significant Ni–O interactions develop for the coadsorbed layer in the range of 130–215 K. On the basis of these results, in conjunction with LEED patterns (*21*), White (*24*) has proposed bonding orientations for CO and H coadsorbed on Ni{100} at low temperatures. At 90 K, H atoms are adsorbed as two states, these being above and below the plane of the outermost Ni atoms. Presumably, these below-plane hydrogens would be located at hollow sites. Chemisorption of CO occurs at atop sites, which, due to the presence of adsorbed H adatoms can easily migrate to bridging or hollow sites. At 140–200 K, the structure rearranges to one comprised of adsorbed H atoms both slightly beneath the Ni surface and CO molecules adsorbed in bridge-bonded and terminally bonded, tilted forms. Following desorption of these Σ-states, CO is strongly held to the surface as it would be in the absence of adsorbed H.

The presence of small coverages of TiO_x adspecies dramatically alters the low-temperature H_2/CO-coadsorption behavior on Ni. On this surface, the following differences were observed compared to the behavior of clean Ni: (a) no low-temperature Σ-states (200–300 K) were observed under any conditions, although enhanced adsorption near 300–350 K suggested some H_2/CO coupling may exist; (b) the most strongly bound hydrogen state, $\beta_2(TiO_x/Ni)$, is *not* displaced to weaker adsorption sites upon adsorption of CO, although, like clean Ni, the β_1 states are completely displaced by CO; (c) the α_1(Ni)–CO state is prevented from reaching saturation in the presence of coadsorbed H; and (d) α_2(Ni)– or $\alpha_1(TiO_x/Ni)$–CO states are not suppressed, but instead are enhanced in the presence of coadsorbed H.

The TPD spectra provide valuable information on which sites are important in terms of competitive adsorption of H_2 and CO. The two most strongly bound H states, $\beta_2(TiO_x/Ni)$ and β_1, and the CO state, α_1(Ni), apparently compete for the same adsorption sites. Specifically, presaturation of the hydrogen $\beta_2(TiO_x/Ni)$ state blocks a fraction of α_1(Ni)–CO states, and CO adsorption displaces β_1–H states to more weakly bound sites. In a previous publication (*11*) we have shown that addition of titania to a Ni surface preferentially converts β_1–H sites to $\beta_2(TiO_x/Ni)$–H sites. Of significance for future discussion is the observation that postdosing a hydrogen-exposed TiO_x/Ni surface with CO does *not* weaken or displace all H-atom adsorption states. This shows that the presence of titania adspecies, as previously suggested, leads to more competitive hydrogen adsorption in the presence of coadsorbed CO. It has been suggested elsewhere (*11*) that the role of titania is to block CO adsorption into strongly bound linear sites atop Ni surface atoms (α_1(Ni) sites) and to subsequently allow adsorption into more weakly bound bridging sites (α_2(Ni)) or multifold

sites ($\alpha_1(TiO_x/Ni)$). This weakening of CO-adsorption strength allows hydrogen to compete more effectively for available adsorption sites.

In the only reported study of the effect of adlayer species on H_2/CO coadsorption, Luftman *et al.* (*19*) investigated the coadsorption of H_2 and CO on potassium-containing Ni surfaces. The presence of small amounts of K ($\theta_K = 0.1$ monolayer) shifted the Σ-state peak temperatures to higher values and attenuated their intensities. For $\theta_K = 0.2$ monolayer, the Σ-states were no longer detectable. The effect of electronegative adatoms on coadsorption behavior has not been reported.

Model Calculations for Nonreactive Coadsorption under Methanation Conditions

On the basis of the UHV experiments described above, one would expect that at typical methanation reaction conditions, the surface concentration of hydrogen on titania-containing nickel surfaces would be higher than on clean nickel surfaces. The magnitude of this difference can be estimated by constructing a competitive adsorption model for CO and H_2. Adsorption and desorption kinetic parameters were obtained from the UHV TPD experiments described in a previous publication (*11*).

A Langmuir adsorption model was developed, in which adsorbed H and CO are in equilibrium with the gas phase:

$$H_{2(g)} + 2* \underset{k_d^H}{\overset{k_a^H}{\rightleftharpoons}} 2H_{(a)} \qquad (1)$$

$$CO_{(g)} + * \underset{k_d^{CO}}{\overset{k_a^{CO}}{\rightleftharpoons}} CO_{(a)} \qquad (2)$$

where * represents unoccupied surface sites, and the subscripts (g) and (a) indicate the gas phase and the adsorbed species, respectively. The following expressions give the equilibrium surface concentration coverages by H and CO in the absence of catalytic reaction:

$$\theta_H = \frac{\left(\frac{k_a^H P_{H_2}}{k_d^H}\right)^{1/2}}{1 + \frac{k_a^{CO} P_{CO}}{k_d^{CO}} + \left(\frac{k_a^H P_{H_2}}{k_d^H}\right)^{1/2}} \qquad (3)$$

$$\theta_{CO} = \frac{\frac{k_a^{CO} P_{CO}}{k_d^{CO}}}{1 + \frac{k_a^{CO} P_{CO}}{k_d^{CO}} + \left(\frac{k_a^H P_{H_2}}{k_d^H}\right)^{1/2}} \qquad (4)$$

where P_i is the partial pressure of species i.

The desorption rate constants can be represented by

$$k_d^H = L^2 \nu_H \exp(-E_d^H/RT) \qquad (5)$$

$$k_d^{CO} = L \nu_{CO} \exp(-E_d^{CO}/RT) \qquad (6)$$

where L is the nickel surface site density, and ν_i and E_d^i are the preexponential factor and the activation energy for desorption of species i, respectively. The second-order preexponential factor ν_H was estimated from an expression for a two-dimensional hard-sphere collision frequency,

$$\nu_H = \tfrac{1}{2} \sigma_0 (\pi RT/m_H)^{1/2} \qquad (7)$$

where σ_0 is the H-adatom collision diameter and m_H the atomic weight of an H atom. Adsorption rates were approximated by the ideal gas expression:

$$k_a^H P_{H_2} = S_0^{H_2} \phi_{H_2} \qquad (8)$$

$$k_a^{CO} P_{CO} = S_0^{CO} \phi_{CO} \qquad (9)$$

where S_0^i is the initial sticking coefficient for gas-phase species i, and ϕ_i is the ideal gas impingement rate,

$$\phi_i = \frac{P_i}{(2\pi m_i RT)^{1/2}}. \qquad (10)$$

Table 1 summarizes the numerical values used in the model for the clean nickel and titania-containing ($\theta_{Ti} = 0.7$ monolayer equivalent) nickel surfaces. Note that these

TABLE 1

Parameters used in the Langmuir Coadsorption Model[a]

Parameter	Ni	TiO_x/Ni
Hydrogen adsorption state	β_1	$\beta_2(TiO_x/Ni)$
$S_0^{H_2}$	0.5	0.001
$E_d^{H_2}$ (kJ · mol^{-1})	86	108
CO adsorption state	α_1(Ni)	$\alpha_1(TiO_x/Ni)$
S_0^{CO}	1.0	0.2
ν_{CO}(s^{-1})	10^{16}	10^{13}
E_d^{CO} (kJ · mol^{-1})	134	91

[a] $\nu_H(T)$ was determined from Eq. (7).

values are those for the most strongly bound, non-activated hydrogen and CO states believed to be associated with Ni sites on the respective surfaces; and, at this titania surface concentration, no CO or H_2 adsorption sites characteristic of clean Ni were evident (*11*). Also note that calculated coverages are based on the Ni area not blocked by titania; i.e., complete monolayer coverages on the respective surfaces are not equivalent in absolute terms. The calculated H- and CO-surface concentrations on the clean Ni surface are plotted versus temperature in Fig. 3 for H_2/CO ratios ranging from 0.5/1 to 10/1. These pressures and temperatures represent the ranges normally used in methanation kinetic studies over nickel. The figure reveals that, in the absence of catalytic reaction, the nickel surface is nearly saturated in CO for all H_2/CO ratios at temperatures less than 570 K. At higher temperatures, the CO surface concentration decreases as molecular CO desorption becomes important. This increases the concentration of vacant sites, which allows an increase in the H-atom surface coverage. Polizotti and Schwarz (*28*) calculated coverage dependences using a similar coadsorption model and reached similar conclusions; however, their model included a hydrogen displacement term proportional to the collision frequency of CO which was not included in the present model.

The presence of titania-surface species alters adsorption strengths and leads to a significantly higher H-adatom coverage based on the available Ni sites. Figure 4 shows the extent of this shift for a H_2/CO ratio of 4 and a total pressure of 1 kPa. At temperatures of 470–650 K, the hydrogen coverage on TiO_x/Ni is one to two orders of magnitude greater than the coverage on clean Ni. Only at temperatures above ~700 K are the surface coverages comparable. An Arrhenius plot of the H-adatom

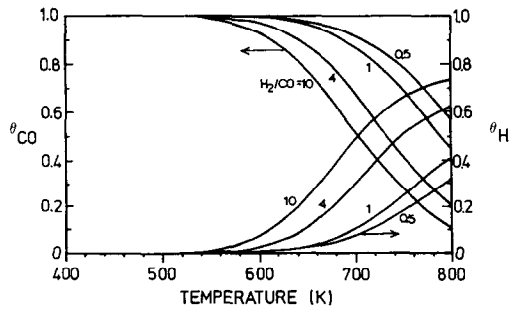

FIG. 3. Calculated variation of CO and H surface coverages on Ni with temperature and H_2/CO ratio at a fixed total pressure of 1 kPa.

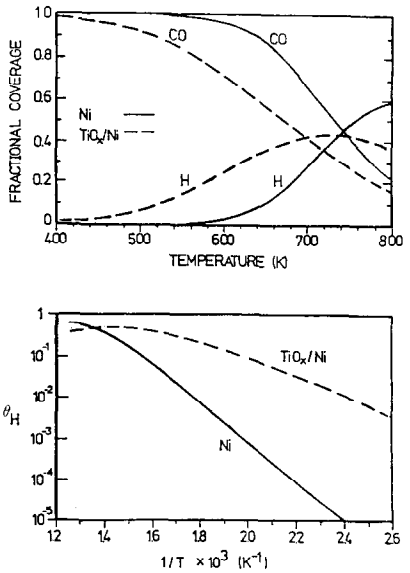

FIG. 4. Comparison of CO and H coverages on Ni and TiO_x/Ni as a function of temperature at a total pressure of 1 kPa and a H_2/CO ratio of 4. θ_H plotted in linear and Arrhenius fashion.

surface concentration versus reciprocal temperature on clean nickel shows an approximately linear relationship at low temperature, with an apparent activation energy of 90 kJ · mol^{-1}. The activation energy decreases at higher temperatures. In the low-temperature regime the temperature dependence is dominated by the change in surface area available for hydrogen chemisorption due to thermal desorption of CO. In the high-temperature limit, hydrogen adsorption/desorption kinetics dominate and cause a maximum in hydrogen coverage at ~700 K. Qualitatively, the calculated H-adatom concentration parallels the experimentally determined temperature dependence of the methanation reaction rate over polycrystalline (*28, 29*) and single crystal nickel (*30, 31*). Thus, it appears that a controlling factor in the observed methanation kinetics is the partial pressure and temperature dependence of the H-adatom surface coverage in the chemisorbed layer. This conclusion is compatible with reaction mechanisms which invoke H-adatom participation in the rate-determining step. This would include both surface carbon hydrogenation and hydrogen-assisted CO dissociation, but would exclude unpromoted CO dissociation as possible rate-limiting steps.

The presence of surface titania gives a surface hydrogen concentration that is somewhat less dependent on temperature, with a low-temperature activation energy of 34 kJ · mol^{-1}. This low value is due primarily to the low extent of hydrogen inhibition by adsorbed CO on the titania-containing surface. In summary, we conclude that the shifts in adsorption strengths caused by titania adspecies lead to significantly greater H-adatom coverages on clean Ni sites under steady-state methanation conditions, and should lead subsequently to higher reaction rates if the rate-limiting step involves surface hydrogen.

TABLE 2

Summary of Rate Constants Used in the Methanation Model

Reaction step	Preexponential factor[a] (molecules · site^{-1} · s^{-1})	E_A (kJ · mol^{-1})
CO dissociation (k_1)	10^{25}	230
C hydrogenation (k_2)	8×10^{14}	145

[a] Includes k_i^0 and site density terms.

Model Calculations for Reactive Coadsorption under Steady-State Methanation Conditions

The calculations described above were performed assuming that adsorbed H and CO did not react on the catalyst surface. A more complete description of the surface concentrations must, however, include not only the hydrogen and carbon monoxide surface concentrations but also the carbon and oxygen that exist on the catalyst surface at steady state. Accordingly, the following set of elementary steps were assumed to occur on the nickel and titania-containing nickel surfaces:

$$H_{2(g)} + 2* \underset{k_d^H}{\overset{k_a^H}{\rightleftharpoons}} 2H_{(a)} \quad (11)$$

$$CO_{(g)} + * \underset{k_d^{CO}}{\overset{k_a^{CO}}{\rightleftharpoons}} CO_{(a)} \quad (12)$$

$$CO_{(a)} + * \xrightarrow{k_1} C_{(a)} + O_{(a)} \quad (13)$$

$$C_{(a)} + H_{(a)} \xrightarrow{k_2} CH_{(a)} \quad (14)$$

$$O_{(a)} + 2H_{(a)} \xrightarrow{\text{fast}} H_2O_{(g)} \quad (15)$$

$$CH_{(a)} + 3H_{(a)} \xrightarrow{\text{fast}} CH_{4(g)}. \quad (16)$$

In this mechanism, adsorbed hydrogen and carbon monoxide are in equilibrium with gas-phase H_2 and CO. Carbon monoxide dissociation is irreversible (*32–34*) and occurs at a rate governed by k_1, θ_{CO}, and θ_*. Removal of surface oxygen is fast so that at steady state, the oxygen-adatom concentration is negligibly small (*30, 31*). Note that a rate-determining step is not assumed, since the rate of CO dissociation is equal to the rate of carbon hydrogenation or methane formation. Goodman *et al.* (*35*) measured independently the rates of carbon forma-

tion from CO dissociation and carbon hydrogenation on Ni{100} and found the rates to be nearly equal. Thus, at steady-state reaction conditions, the methanation rate and surface carbon level are determined by a balance between the C formation and removal rates. On the basis of these assumptions, the following expression describes the methanation rate at steady state:

$$r_{CH_4} = \frac{k_1 K_A^{CO} P_{CO}}{\left\{1 + K_A^{CO} P_{CO} + \frac{k_1 K_A^{CO} P_{CO}}{k_2 (K_A^H P_{H_2})^{1/2}} + (K_A^H P_{H_2})^{1/2}\right\}^2} \quad (17)$$

where K_A^{CO} and K_A^H are the equilibrium constants for CO and hydrogen adsorption, and are equal to $K_0^{CO} \exp(-\Delta H_A^{CO}/RT)$ and $K_0^H \exp(-\Delta H_A^H/RT)$, respectively. Heats of adsorption, ΔH_A^{CO} and ΔH_A^H, are equal in magnitude to the respective activation energies for desorption of CO and hydrogen, since these molecules adsorb on nickel via nonactivated processes.

Adsorption constants were determined as described previously. Activation energies for CO dissociation and carbon hydrogenation were obtained from the literature. Tomanek and Bennemann (*36*) have estimated an activation energy barrier of 230 kJ · mol^{-1} for CO dissociation on a Ni{111} surface using LCAO–MO methods. Rosei *et al.* (*37*) have measured an *apparent* CO dissociation activation energy on Ni{110} of 96 kJ · mol^{-1}. Correcting for the heat of adsorption of CO at low coverage (−134 kJ · mol^{-1}) leads to a value for the true activation energy of 230 kJ · mol^{-1}, in excellent agreement with the theoretical results. Accordingly, a value of 230 kJ · mol^{-1} was used in the model. Experimentally measured activation energies for carbon hydrogenation on nickel, corrected for the hydrogen heat of adsorption at low hydrogen coverage (−86 kJ · mol^{-1}/2), range from 135 to 148 kJ · mol^{-1} (*35, 38*). Note that these values were obtained under isothermal conditions, and are considerably larger than values measured under temperature-programmed conditions (*39, 40*), wherein apparent activation energies from 40 to 70 kJ · mol^{-1} (true energies from 83 to 113 kJ · mol^{-1}) were determined. It is believed that the values measured under isothermal conditions may be the more appropriate values, and hence a value of 145 kJ · mol^{-1} was used in the model. Preexponential factors for k_1 and k_2 were chosen to give a methanation turnover frequency (TOF) equal to ~0.04 s^{-1} at 550 K and $H_2/CO = 4$ (*31, 38*), a value reported for both single crystal Ni and alumina-supported Ni. Table 2 summarizes the parameters used.

With this model, it can be shown that changes in heats of adsorption of the reactants H_2 and CO on Ni due to the presence of titania surface species significantly alter methanation behavior. The effects of titania adspecies are illustrated with the aid of Figs. 5 and 6, which compare the temperature dependence of specific methanation activity and surface concentrations of CO, H, and C for a clean Ni surface and a titania-containing Ni surface. Figure 5 shows that the presence of titania adspecies in-

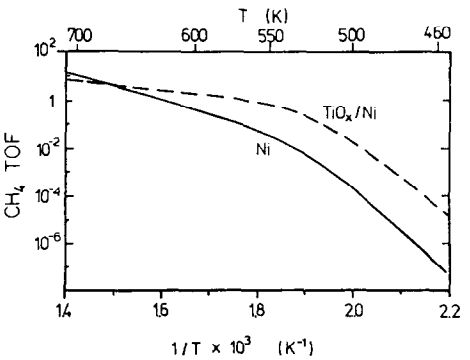

FIG. 5. Comparison of the methanation turnover frequency over clean Ni and titania-containing Ni based on model calculations. Total reactant pressure 160 Pa; $H_2/CO = 4$.

creases the steady-state rate of CO methanation for all temperatures below ~650 K. Three separate regimes are evident in the kinetic behavior over both surfaces; these can be differentiated by comparison with Fig. 6. At temperatures below about 480 K, the surface coverage by CO dominates, with few sites populated by carbon or hydrogen. The apparent activation energy in this regime is high. In the limit of high θ_{CO}, the rate expression becomes

$$r_{CH_4}\Big|_{\substack{\lim \\ \theta_{CO}\to 1}} = \frac{k_1}{K_A^{CO}P_{CO}} \tag{18}$$

and the apparent activation energy is

$$E_{app}\Big|_{\substack{\lim \\ \theta_{CO}\to 1}} = E_1 - \Delta H_A^{CO}. \tag{19}$$

This gives apparent activation energies of ~360 and 320 kJ · mol^{-1} on the Ni and TiO_x/Ni surfaces, respectively.

At high temperatures, i.e., above ~570 K, the surfaces are nearly completely covered with surface carbon. In this regime, the apparent activation energy, based on the limiting rate expression

$$r_{CH_4}\Big|_{\substack{\lim \\ \theta_C\to 1}} = \frac{k_2^2 K_A^H P_{H_2}}{k_1 K_A^{CO} P_{CO}} \tag{20}$$

is equal to

$$E_{app}\Big|_{\substack{\lim \\ \theta_C\to 1}} = 2E_2 + \Delta H_A^H - E_1 - \Delta H_A^{CO}. \tag{21}$$

This gives apparent values of 108 kJ · mol^{-1} on clean Ni and 43 kJ · mol^{-1} on TiO_x/Ni.

In the intermediate regime (480–570 K), neither CO nor C dominate, and the apparent activation energy gradually shifts from high to low values with increasing temperature. Note that the model predicts shifts in apparent activation energies, dependent on the temperature measurement range, without invoking a change in mechanism or the nature of a rate-limiting step. Since neither carbon formation nor removal are rate determining, surface carbon concentration is particularly sensitive to reactant partial pressures and temperatures in the intermediate temperature regime.

Examination of the variations of surface coverages at different temperatures, Fig. 6, shows that the higher methanation activity of the TiO_x/Ni surface can be attributed to lower coverages of molecularly adsorbed CO and significantly higher hydrogen adatom coverage. In the low-temperature regime, the presence of titania adspecies decreases θ_{CO} by about 10%; this represents a significant increase in the surface area available for hydrogen adsorption. For temperatures from 450 to 500 K, θ_H on TiO_x/Ni is about two orders of magnitude higher than on clean Ni (note that the values for nickel have been multiplied by a factor of 20 in the lower half of Fig. 6). This leads to an increase in the methanation turnover frequency by two orders of magnitude, assuming that the rate constants for carbon hydrogenation and CO dissociation are unchanged by the presence of TiO_x species. Note that in this regime the predicted results are controlled by the CO heats of adsorption and are relatively insensitive to values used for hydrogen heats of adsorption.

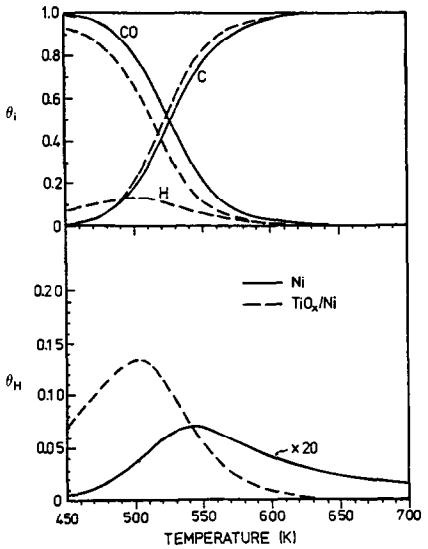

FIG. 6. Surface coverages for clean Ni and titania-containing Ni as a function of temperature. Total reactant pressure 160 Pa; $H_2/CO = 4$.

At higher temperatures, carbon covers a greater fraction of the surface not occupied by CO, reducing the fractional coverage by hydrogen. This reduces the differences between the TiO_x/Ni and clean Ni surfaces. Nonetheless, at 550 K, a temperature commonly chosen for activity comparisons, the turnover frequency over the TiO_x/Ni surface is about one order of magnitude higher than that over the clean Ni surface.

In summary, the results of this model are consistent with the previous (nonreactive) Langmuir coadsorption model which predicted that the presence of titania adspecies leads to more competitive hydrogen adsorption and thereby increases the surface H-adatom coverage (by up to two orders of magnitude). This effect of titania exists over a wide range of experimental conditions representative of those used in methanation studies over model nickel and high-surface-area supported-nickel catalysts (i.e., 0.01–1 atm, 450–650 K, H_2/CO = 10–1). It thus appears that lower CO-adsorption strengths lead to higher methanation activities. This conclusion is supported by the work of Campbell and Goodman (*41*) who showed that the presence of potassium adatoms decreased the rate of methane formation on Ni{100}. Kiskinova (*42*) had previously demonstrated that K adatoms increase the heat of adsorption on nickel as well as enhance CO dissociation probability.

Consequences of Model Calculations for Methanation

As discussed above, we favor a model wherein neither CO dissociation nor carbon hydrogenation is rate determining. Instead, the overall reaction rate is determined by a balance between these two competing processes, as previously proposed by Goodman and co-workers (*30, 31*). For this model to be valid over both clean nickel and titania-containing nickel, it must exhibit the following trends observed for methanation over titania-supported nickel catalysts relative to traditional nickel catalysts (*40, 43, 44*): (a) one to two orders of magnitude higher methanation activity, (b) a higher apparent activation energy of methanation, (c) no change in the CO partial pressure dependence and an increase in the H_2 partial pressure dependence, (d) greater selectivity to higher hydrocarbons, and (e) greater resistance to deactivation. In the discussion to follow it is demonstrated that the proposed methanation model can adequately explain each of these trends, with the exception of the increase in H_2 partial pressure dependence.

(*a*) *Activity*. Methanation turnover frequencies for titania-supported nickel are generally one order of magnitude higher than alumina-supported nickel and two orders of magnitude higher than silica-supported nickel (*43, 44*). Goodman and Kelley (*31*) compared specific activities for single crystal Ni{100} and Ni{111} with published data on high surface area alumina-supported Ni and concluded that the activities on these different surfaces were identical within experimental error. Thus, it appears that nickel/titania catalysts are about one order of magnitude more active than supported "clean" nickel crystallites; the use of silica as a support leads to a reduction in activity of the nickel particles. Deleterious effects of silica have previously been observed in other systems (e.g., *45*).

A factor of 10 increase in activity can be readily explained by the presence of titania adspecies, which increase the steady-state hydrogen-adatom coverage. At a given reaction temperature, the steady-state CO coverage is lower on the titania-containing Ni, consistent with the observations of Vannice on various supported Pt catalysts using *in situ* infrared spectroscopy (*12*). As previously suggested by Jiang *et al.* (*44*), titania adspecies also lead to a higher concentration of active carbon on the nickel surface.

Note that the higher methanation activity can be explained entirely by changes in heats of adsorption on *nickel* sites. It is not necessary to invoke a reaction mechanism

in which the reaction takes place at special sites created at the titania–metal interface where C–O bond breaking takes place (although the results of this model do not preclude this possibility). Neither is it necessary to invoke a new mechanism, nor a shift in rate-limiting steps; the reaction sequence and rate constants were kept constant throughout. The work of Ozdogan *et al.* (*40*) suggested that the rate of carbon hydrogenation under temperature-programmed conditions, in the absence of coadsorbed CO, was independent of the support for nickel supported on SiO_2, SiO_2–Al_2O_3, Al_2O_3, and TiO_2. More recently Bartholomew and Vance (*46*) have used isothermal thermogravimetry to show that the activation energy for carbon hydrogenation is independent of support, although turnover frequencies varied in the ratio 8/2/1 for nickel supported on TiO_2, Al_2O_3, and SiO_2, respectively. Based on theoretical predictions (*36*) and experimental measurements (*47*) for electronegative adatoms on Group VIII metals, it is expected that titania adspecies might decrease the rate of CO dissociation on nickel. A decrease in the dissociation rate constant by a factor of 10 would still give a higher net methanation activity for the TiO_x/Ni surface, while shifting the steady-state carbon coverage to somewhat lower values.

(*b*) *Activation energy.* On the clean Ni surface, the model predicts that the apparent activation energy shifts from a high value on a carbon monoxide covered surface at low temperatures to a low value on a carbon-covered surface at high temperatures. Qualitatively, this behavior has been observed independent of support material. Kelley *et al.* (*29*) compared data collected by various researchers over a variety of nickel-based catalysts and noted a correlation between measured activation energy and the temperature range of the measurement. Values near 130 kJ · mol^{-1} at 470 K decreased smoothly to values near 80 kJ · mol^{-1} at 570 K. Weatherbee and Bartholomew (*48*) recently observed a decrease in activation energy from 130 kJ · mol^{-1} at 470 K to 70 kJ · mol^{-1} at 620 K for measurements performed over a silica-supported nickel catalyst. The model results show that this type of behavior can be understood without assuming a change in mechanistic steps or the nature of the rate-limiting reaction step. Instead, the two extremes in apparent activation energy can be attributed to different surface concentrations of carbon and CO. Studies using isotopic transient tracing techniques (*49–51*) give results in agreement with the model, showing that at low temperatures the surface is covered mostly with CO, while at higher temperatures carbidic carbon and partially hydrogenated carbon (CH_x species) dominate.

The high-temperature limiting value of 108 kJ · mol^{-1} determined from the model is typical of the value reported for single crystal nickel (*30, 31, 35, 52*), and alumina-supported nickel (*38*) at high temperatures. Lower values would be obtained if the model accounted for weakening of CO adsorption with increasing carbon coverage. Low-temperature limiting values are dependent on the assumed value for the CO dissociation activation energy. If values lower than the assumed 230 kJ · mol^{-1} are used, then the range of the transition regime shifts to lower temperatures and the low-temperature limiting apparent activation energy decreases accordingly. The temperature range of the transition region is also dependent on the assumed preexponential factors. Thus, the numerical values predicted by the model in the low-temperature and transition regimes cannot be viewed quantitatively. Nonetheless, the trends illustrated can be used to explain the observed higher activation energies for titania-supported catalysts.

At a given temperature the slopes of the two activity versus temperature curves in Fig. 5 are nearly equivalent, with the curve for TiO_x/Ni actually having a lower slope than that for Ni. However, it should be noted that due to mass and heat transfer

limitations and the higher inherent activity of titania-containing samples, kinetic measurements over these samples are generally performed at temperatures 40–70 K lower (and extrapolated to higher temperatures) than alumina- or silica-supported nickel samples. If activation energies are determined at equivalent methanation turnover numbers near, for example, 0.1 molecules $CH_4 \cdot site^{-1} \cdot s^{-1}$, an apparent activation energy of ~ 105 kJ $\cdot$ mol^{-1} results from evaluation near 570 K on the clean nickel surface, whereas a value of 194 kJ $\cdot$ mol^{-1} results from evaluation near 500 K on the titania-containing nickel surface.

(c) *Partial pressure dependence.* In the limit of high carbon coverage (high temperature), the derived expression for the steady-state methanation rate reduces to

$$r_{CH_4}\Big|_{\substack{\lim \\ \theta_C \to 1}} \approx \frac{k_2^2 K_A^H}{k_1 K_A^{CO}} P_{CO}^{-1} P_{H_2}^{+1} \qquad (22)$$

and in the limit of low-carbon coverage (low temperature) it reduces to

$$r_{CH_4}\Big|_{\substack{\lim \\ \theta_C \to 0}} \approx \left\{\frac{k_1}{K_A^{CO}}\right\} P_{CO}^{-1}. \qquad (23)$$

Note that the CO partial pressure dependence is approximately -1 over the full range of surface coverages, and it is not dependent on whether the Ni surface is clean or titania covered. This invariance of the CO pressure dependence agrees with experimental measurements, although in general the measured reaction order is in the range from -0.3 to -0.5.

At high-carbon coverages, the observed hydrogen pressure dependence arises from the carbon-coverage term in the Langmuir–Hinshelwood expression. Thus, a higher carbon coverage generally leads to a greater dependence of the rate on P_{H_2}. In the transition temperature regime the carbon coverage on TiO_x/Ni is somewhat higher than the corresponding coverage on Ni for identical reaction conditions; this tends to give a higher H_2 partial pressure dependence. However, hydrogen adsorption/desorption contributes a non-negligible negative pressure dependence, and for certain reaction conditions can lead to a lower P_{H_2} dependence over TiO_x/Ni than over clean nickel. For example, at 540 K the model predicts that the methanation turnover frequency on clean Ni is proportional to $P_{H_2}^{+0.5}$ at a partial pressure of CO equal to 133 Pa and H_2/CO ratios from 1 to 10. For identical conditions, the hydrogen partial pressure dependence of the rate over TiO_x/Ni decreases from $+0.68$ to 0.44 as the H_2/CO ratio increases from 1 to 10. Thus, the model does not completely describe the experimentally observed trend that the hydrogen reaction order is higher over titania-supported nickel.

A minor modification to the model could lead to increases in the P_{H_2} dependence over TiO_x/Ni. If we increase the assumed number of hydrogen atoms involved in the rate-limiting step in carbon hydrogenation, then this would lead to a substantial increase in the hydrogen-pressure dependence. In the proposed model, one H atom was involved, and subsequent hydrogen addition steps were assumed to be kinetically insignificant. Clearly, this is a limiting assumption, as all forms of partially hydrogenated carbon (CH, CH_2, CH_3) are present in measurable amounts on supported-nickel crystallites (*49, 50, 53*).

(*d*) *Selectivity.* The model predicts somewhat higher steady-state carbon coverages for the titania-containing surface relative to the clean surface. This result is not obvious, since one might generally expect that increased H-adatom coverages should lead to lower C coverages. One must remember, however, that in the model CO dissociation and C hydrogenation are balanced, and for the titania-containing surface, the rates of both reactions increase proportionally. This behavior has been experimentally observed by Bartholomew and Vance, who independently measured the rates of CO dissociation in the presence of hydrogen and the rate of C hydrogenation and found

both rates to be higher over titania-supported Ni relative to alumina or silica-supported Ni (*46*).

Higher carbon coverages shift the product distribution on Ni{100} toward higher hydrocarbons (*41*). Thus, if carbon chain growth through carbidic carbon "polymerization" is rate limiting (*54*), more carbon present on the surface will increase the probability for reaction events leading to C–C bond formation.

The work of Kelley and Semancik (*55*) provides an alternative explanation for chain growth in CO hydrogenation over nickel. Higher hydrocarbon production was found to be a strong function of the CO partial pressure, and it was thus proposed that higher hydrocarbon chain growth occurs through CO insertion into the metal–carbon bond of an adsorbed CH_x intermediate. The CO involved in this step must be strongly pressure dependent, thus excluding the strongly bound α_1–CO admolecules at atop sites which are essentially pressure independent. More weakly bound α_2–CO molecules at hollow and bridging sites are pressure dependent; moreover, as demonstrated previously (*11*), the presence of titania adspecies enhances the coverage of these weaker α_2–CO states. These titania adspecies block CO from adsorbing on atop sites, and thereby enhance the populations of CO at hollow or bridging sites. Thus, if these weakly bound CO molecules are directly involved in the formation of higher hydrocarbons, one would expect an enhancement in selectivity to higher hydrocarbons for titania-containing nickel surfaces.

(*e*) *Deactivation.* Deactivation of nickel methanation catalysts may occur, for example, through particle sintering or inactive (graphitic) carbon deposition. Sintering is most severe in CO-containing atmospheres at low temperatures, conditions under which particle growth occurs via transport of volatile nickel carbonyls (*56*). The rate of $Ni(CO)_4$ formation on titania-supported nickel is significantly slower than the rate over Ni single crystals (*57*) or nickel supported on silica or alumina (*43*). This inhibition may be directly related to the weakening of the CO-adsorption strength induced by the presence of titania adspecies on the nickel particles.

Surface graphitic deposits block active sites (*30, 58, 59*). Jiang *et al.* (*44*) have suggested that one role of titania surface species is to minimize the accumulation of graphitic carbon on the surfaces of the nickel particles. Goodman *et al.* (*30*) have shown that formation of graphite on a nickel single crystal in an H_2/CO atmosphere requires both a critical temperature (~650 K) and a prerequisite surface active carbon level ($\theta_C \sim 0.5$ monolayer). For hydrogen pressures sufficient to minimize carbon accumulation, the catalyst surface could be maintained free of graphite for temperatures up to 800 K. Minimization of graphite formation may therefore be related to the higher hydrocarbon adatom coverage on titania-containing nickel surfaces under steady-state methanation conditions.

CONCLUSIONS

Study of the coadsorption/desorption behavior of H_2 and CO on nickel and titania-containing nickel surfaces under UHV conditions confirmed that these reactant molecules compete for the same sites. The presence of titania adspecies blocks CO adsorption at strongly bound sites and allows adsorption into more weakly bound sites. In addition, the presence of titania on nickel increases the strength of hydrogen adsorption. This weakening of CO adsorption and strengthening of hydrogen adsorption allows hydrogen to compete more effectively for nickel-adsorption sites.

Model calculations performed for moderate pressures (0.1 to 1.0 kPa) and temperatures (450–700 K) suggest that the observed shifts in CO and hydrogen adsorption strength should lead to H-adatom surface concentrations which are one to two orders of magnitude higher over a titania-containing surface under steady-state methanation

conditions, compared to clean nickel. Moreover, assuming a methanation mechanism wherein neither CO dissociation nor C hydrogenation is rate limiting, the calculations showed that the higher hydrogen adatom coverage leads directly to a higher methanation turnover frequency.

Thus, we have shown that the presence of titania species on the surfaces of nickel particles can qualitatively explain methanation over titania-supported catalysts which exhibit so-called strong metal–support interactions. Importantly, the key features of methanation could be reproduced by a model wherein the reaction mechanism was preserved between the clean nickel and the titania-containing surfaces. The kinetic parameters for CO dissociation and carbon hydrogenation were also held constant; only the heats of adsorption of carbon monoxide and hydrogen were varied. Accordingly, the effects of strong metal–support interactions on methanation behavior can be rationalized in terms of more competitive hydrogen adsorption on *nickel* sites; i.e., the participation of special interfacial CO dissociation sites need not be invoked. This does not imply that the metal–titania interface is not important to the overall chemistry of the surface. Indeed, the increase in the heat of adsorption for hydrogen can be attributed to adsorption at interfacial sites in titania-supported Pt catalysts (*60, 61*), as we have previously suggested for titania-containing Ni surfaces (*11*).

ACKNOWLEDGMENTS

The financial support of Eastman Kodak through a fellowship for one of us (GBR) is gratefully acknowledged. We also thank the National Science Foundation for partial funding of this research.

REFERENCES

1. Santos, J., Phillips, J., and Dumesic, J. A., *J. Catal.* **81,** 147 (1983).
2. Resasco, D. E., and Haller, G. L., *J. Catal.* **82,** 279 (1983).
3. Mériaudeau, P., Dutel, J. F., Dufaux, M., and Naccache, C., *Stud. Surf. Sci. Catal.* **11,** 95 (1982).
4. Jiang, X. Z., Hayden, T. F., and Dumesic, J. A., *J. Catal.* **83,** 168 (1983).
5. Chung, Y.-W., Xiong, G., and Kao, C.-C., *J. Catal.* **85,** 237 (1984).
6. Sadeghi, H. R., and Henrich, V. E., *J. Catal.* **87,** 279 (1984).
7. Simoens, A. J., Baker, R. T. K., Dwyer, D. J., Lund, C. R. F., and Madon, R. J., *J. Catal.* **86,** 359 (1984).
8. Raupp, G. B., and Dumesic, J. A., *J. Phys. Chem.* **88,** 660 (1984).
9. Vannice, M. A., and Sudhaker, C., *J. Phys. Chem.* **88,** 2429 (1984).
10. Takatani, S., and Chung, Y.-W., *J. Catal.* **90,** 75 (1984).
11. Raupp, G. B., and Dumesic, J. A., *J. Catal.*, in press.
12. Vannice, M. A., Twu, C. C., and Moon, S. H., *J. Catal.* **79,** 70 (1983).
13. Bertolini, J. C., and Imelik, B., *Surf. Sci.* **80,** 586 (1979).
14. Goodman, D. W., Yates, J. T., Jr., and Madey, T. E., *Surf. Sci.* **93,** L135 (1980).
15. Koel, B. E., Peebles, D. E., and White, J. M., *Surf. Sci.* **125,** 709 (1983).
16. Koel, B. E., Peebles, D. E., and White, J. M., *J. Vac. Sci. Technol.* **20**(3), 889 (1982).
17. Koel, B. E., Peebles, D. E., and White, J. M., *Surf. Sci.* **107,** L367 (1981).
18. Peebles, D. E., Peebles, H. C., Belton, D. N., and White, J. M., *Surf. Sci.* **134,** 46 (1983).
19. Luftman, H. S., Sun, Y.-M., and White, J. M., *Surf. Sci.* **140,** L259 (1984).
20. Koel, B. E., Peebles, D. E., and White, J. M., *Surf. Sci.* **125,** 739 (1983).
21. Peebles, H. C., Peebles, D. E., and White, J. M., *Surf. Sci.* **125,** L87 (1983).
22. Mitchell, G. E., Gland, J. L., and White, J. M., *Surf. Sci.* **131,** 167 (1983).
23. Craig, J. H., Jr., *Surf. Sci.* **141,** L291 (1984).
24. White, J. M., *J. Phys. Chem.* **87,** 915 (1983).
25. Udovic, T. J., and Dumesic, J. A., *J. Catal.* **89,** 314 (1984).
26. Kim, Y., Peebles, H. C., and White, J. M., *Surf. Sci.* **114,** 363 (1982).
27. Williams, E. D., Thiel, P. E., Weinberg, W. H., and Yates, J. T., Jr., *J. Chem. Phys.* **72,** 3496 (1982).
28. Polizotti, R. S., and Schwarz, J. A., *J. Catal.* **77,** 1 (1982).
29. Kelley, R. D., Madey, T. E., Revesz, K., and Yates, J. T., Jr., *Appl. Surf. Sci.* **1,** 266 (1978).
30. Goodman, D. W., Kelley, R. D., Madey, T. E., and Yates, J. T., Jr., *J. Catal.* **63,** 226 (1980).
31. Goodman, D. W., and Kelley, R. D., *Surf. Sci.* **123,** L743 (1982).
32. Goodman, D. W., and Yates, J. T., Jr., *J. Catal.* **82,** 255 (1983).

33. Biloen, P., Helle, J. N., and Sachtler, W. M. H., *J. Catal.* **58,** 95 (1979).
34. Araki, M., and Ponec, V., *J. Catal.* **44,** 439 (1976).
35. Goodman, D. W., Kelley, R. D., Madey, T. E., and White, J. M., *J. Catal.* **64,** 479 (1980).
36. Tomanek, D., and Bennemann, K. H., *Surf. Sci.* **127,** L111 (1983).
37. Rosei, R., Ciccacci, F., Memeo, R., Marianna, C., Caputi, L. S., and Papagno, L., *J. Catal.* **83,** 19 (1983).
38. Vannice, M. A., *Catal. Rev. Sci. Eng.* **14,** 153 (1976).
39. McCarty, J. G., and Wise, H., *J. Catal.* **57,** 406 (1979).
40. Ozdogan, S. Z., Gochis, P. D., and Falconer, J. L., *J. Catal.* **83,** 257 (1983).
41. Campbell, C. T., and Goodman, D. W., *Surf. Sci.* **123,** 413 (1982).
42. Kiskinova, M. P., *Surf. Sci.* **111,** 584 (1981).
43. Vannice, M. A., and Garten, R. L., *J. Catal.* **56,** 236 (1979).
44. Jiang, X.-Z., Stevenson, S. A., and Dumesic, J. A., *J. Catal.* **91,** 11 (1985).
45. Lund, C. R. F., and Dumesic, J. A., *J. Catal.* **76,** 93 (1982).
46. Bartholomew, C. H., and Vance, C. K., *J. Catal.* **91,** 78 (1985).
47. Kiskinova, M., and Goodman, D. W., *Surf. Sci.* **108,** 64 (1981).
48. Weatherbee, G. D., and Bartholomew, C. H., *J. Catal.* **77,** 460 (1982).
49. Happel, J., Suzuki, I., Kokayeff, P., and Fthenakis, V., *J. Catal.* **65,** 59 (1980).
50. Happel, J., Cheh, H. Y., Otarod, M., Ozawa, S., Severdia, A. J., Yoshida, T., and Fthenakis, V., *J. Catal.* **75,** 314 (1982).
51. Biloen, P., Helle, J. N., van den Berg, F. G. A., and Sachtler, W. M. H., *J. Catal.* **81,** 450 (1983).
52. Kao, C. C., Tsai, S.-C., and Chung, Y.-W., *J. Catal.* **73,** 136 (1982).
53. Otarod, M., Ozawa, S., Yin, F., Chew, M., Cheh, H. Y., and Happel, J., *J. Catal.* **84,** 156 (1983).
54. Bell, A. T., *Catal. Rev. Sci. Eng.* **23,** 203 (1981).
55. Kelley, R. D., and Semancik, S., *J. Catal.* **84,** 248 (1983).
56. Shen, W. M., Dumesic, J. A., and Hill, C. G., Jr., *J. Catal.* **68,** 152 (1981).
57. Greiner, G., and Menzel, D., *J. Catal.* **77,** 382 (1982).
58. McCarty, J. G., and Madix, R. J., *Surf. Sci.* **54,** 121 (1976).
59. Wentrcek, P. R., McCarty, J. G., Wood, B. J., and Wise, H., *Amer. Chem. Soc. Div. Fuel Chem. Prepr.* **21,** 52 (1976).
60. Beck, D. D., and White, J. M., *J. Phys. Chem.* **88,** 2764 (1984).
61. Beck, D. D., Bawagan, A. O., and White, J. M., *J. Phys. Chem.* **88,** 2771 (1984).